

# Perturbation of Fluid Dynamics Properties of Water Molecules during G Protein-Coupled Receptor–Ligand Recognition: The Human A<sub>2A</sub> Adenosine Receptor as a Key Study

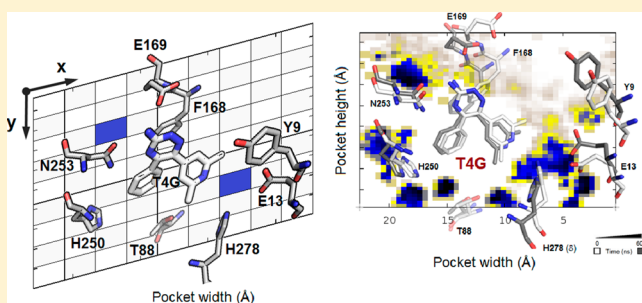
Davide Sabbadin,<sup>†,‡</sup> Antonella Ciancetta,<sup>†</sup> and Stefano Moro<sup>\*,†</sup>

<sup>†</sup>Molecular Modeling Section (MMS), Dipartimento di Scienze del Farmaco, Università di Padova, via Marzolo 5, 35131 Padova, Italy

<sup>‡</sup>Syngenta Crop Protection AG, Schaffhauserstrasse 101, 4332 Stein, Switzerland

Supporting Information

**ABSTRACT:** Recent advances in structural biology revealed that water molecules play a crucial structural role in the protein architecture and ligand binding of G protein-coupled receptors. In this work, we present an alternative approach to monitor the time-dependent organization of water molecules during the final stage of the ligand–receptor recognition process by means of membrane molecular dynamics simulations. We inspect the variation of fluid dynamics properties of water molecules upon ligand binding with the aim to correlate the results with the binding affinities. The outcomes of this analysis are transferred into a bidimensional graph called water fluid dynamics maps, that allow a fast graphical identification of protein “hot-spots” characterized by peculiar shape and electrostatic properties that can play a critical role in ligand binding. We hopefully believe that the proposed approach might represent a valuable tool for structure-based drug discovery that can be extended to cases where crystal structures are not yet available, or have not been solved at high resolution.



## INTRODUCTION

Water is a essential component of biological systems. Its crucial effect on protein structure, dynamics, as well as on protein-mediated substrate transformation has been widely demonstrated.<sup>1</sup> Moreover, in the last 20 years, the role played by water molecules in the molecular recognition of small molecular entities by receptors has been increasingly recognized.<sup>2–4</sup> Nevertheless, the effect of water molecules on ligand binding has only recently started to be considered in drug discovery processes.<sup>5–7</sup> Nowadays, it is generally thought that water molecules contribute to protein–ligand binding in two ways: they can either stabilize the complex by forming additional hydrogen bond networks,<sup>8</sup> or can be displaced by the ligand once the complex is formed.<sup>9,10</sup> In the first case, the contribution to ligand binding is of pure enthalpic nature, whereas in the latter case, the contribution arises from the entropic gain of the release of ordered water molecules into the bulk associated with the enthalpic gain of newly established protein–ligand interactions.<sup>11</sup>

The main issue concerning the incorporation of the effect of water molecules in drug design is the ability to distinguish between water molecules that mediate protein–ligand interactions and those that can be targeted for displacement. X-ray diffraction has long been used to locate water molecules in protein binding sites. However, the structure resolution represents a limiting factor for the detection of a consistent number of water molecules, and more frequently, crucial

hotspots cannot be caught due to insufficient resolution.<sup>12</sup> It is therefore evident that complementary methods are needed to locate water molecules in protein binding sites and predict their likelihood of being displaced. Over the years, several computational techniques based on different backgrounds have been developed: in the drug discovery scenario, there are currently available fast methods such as GRID,<sup>13</sup> knowledge-based,<sup>14–16</sup> empirical,<sup>17</sup> and machine-learning-based approaches,<sup>18</sup> as well as more computationally expensive approaches relying on molecular dynamics (MD) simulations based on statistical mechanics,<sup>19</sup> double decoupling method,<sup>20</sup> free energy perturbation,<sup>21</sup> and inhomogeneous fluid solvation theory.<sup>22–26</sup>

In the present work, we introduce an alternative approach based on the monitoring of the time-dependent organization of water clusters during the final stage of the ligand recognition process by means of MD simulations. Basically, our approach inspects the variation of fluid dynamics properties of water molecules acted by the binding event with the aim to correlate the results with the binding affinities of different ligands. To analyze this complex time-dependent process, we elaborated a protocol to detect structural water molecules inside the orthosteric binding site of the receptor. The results of this analysis are then collected in a bidimensional graph that we called water fluid dynamics (WFD) map.

**Received:** July 4, 2014



Table 1. Structurally Related 1,2,4-Triazine Derivatives

Compound	Structure	SlogP (o/w)	vdW volume ( $\text{\AA}^3$ )	MW (Da)	pK <sub>i</sub>	K <sub>D</sub>
<b>1</b> 1,2,4-triazin-3-amine		-0.34	115.50	96.093	ND	ND
<b>2 (4a)</b> diphenyl-1,2,4-triazine-3-amine		3.49	345.45	248.28	6.93	$>1 \cdot 10^0$
<b>3 (4d)</b> 6-(3,5-dimethylphenyl)-5-phenyl-1,2,4-triazin-3-amine		4.20	394.30	276.34	7.67	ND
<b>4</b> 5-phenyl-6-(pyridin-4-yl)-1,2,4-triazin-3-amine		2.26	336.37	249.27	ND	ND
<b>5 (4g)</b> 6-(2,6-dimethylpyridin-4-yl)-5-phenyl-1,2,4-triazin-3-amine		2.86	385.23	277.33	8.11	$1.15 \cdot 10^{-2}$

As test case, we have selected the human adenosine A<sub>2A</sub> receptor (hA<sub>2A</sub> AR), which has been recently crystallized with several ligands, both agonists and antagonists, characterized by different receptor binding affinities. The presence of ordered clusters of water molecules in the proximity of highly conserved motifs in class A GPCRs, to which adenosine receptors (ARs) belong, suggested their structural role in stabilizing intra- and interhelical interactions,<sup>26</sup> and water dynamics revealed to play a pivotal role in both rhodopsin activation and signaling.<sup>27,28</sup> Moreover, the recent high-resolution crystal structure of hA<sub>2A</sub> ARs has highlighted the active role of water molecules in the ligand–receptor recognition process.<sup>29</sup> In particular, the effect of the perturbation of clusters of water molecules in ligand binding has been recently investigated by highlighting that precise water modeling is essential not only for accurate binding free energy predictions but also for a better understanding of ligand binding kinetics.<sup>30</sup>

Specifically, we have chosen five crystal structures of the hA<sub>2A</sub> AR in complex with four strong binders such as 4-(2-(7-amino-2-(2-furyl)(1,2,4)triazolo(2,3-*a*)(1,3,5)triazin-5-yl-amino)-ethyl)phenol, ZM 241385 ( $\text{pK}_D = 9.18 \pm 0.00$ ,<sup>31</sup> PDB ID: 3EML<sup>32</sup>); 6-(2,6-dimethylpyridin-4-yl)-5-phenyl-1,2,4-triazin-3-amine, T4G ( $\text{pK}_D = 8.9 \pm \text{n.d.}$ ,<sup>31</sup> PDB ID: 3UZA<sup>33</sup>); 4-(3-amino-5-phenyl-1,2,4-triazin-6-yl)-2-chlorophenol, T4E ( $\text{pK}_D = 9.6 \pm \text{n.d.}$ ,<sup>31</sup> PDB ID: 3UZC<sup>33</sup>); NECA: *N*-ethyl-5'-carboxamido adenosine ( $\text{pK}_D = 7.00 \pm 0.1$ ,<sup>31</sup> PDB ID: 2YDV<sup>34</sup>) and the weaker binder caffeine ( $\text{pK}_D = 5.31 \pm 0.44$ ,<sup>31</sup> PDB ID: 3RFM<sup>31</sup>). In addition, we also investigated the time-dependent organization of water clusters within the orthosteric binding pocket of the apo-state of the receptor and its ligand-bound state, focusing on various structurally related 1,2,4-triazine derivatives antagonist at the hA<sub>2A</sub> AR. Ligands were obtained by virtual modifications of the 6-(2,6-dimethylpyridin-4-yl)-5-phenyl-1,2,4-triazin-3-amine and re-

ported in Table 1. Most of the hA<sub>2A</sub> AR antagonists considered in this study have been recently synthesized and reported in literature.<sup>33</sup>

## METHODS

**Computational Facilities.** All computations were performed on a hybrid CPU/GPU cluster. In particular, molecular docking simulations have been carried out using 8 Intel Xeon E5620 CPU cluster, whereas membrane molecular dynamics simulation have been performed with a 4 NVIDIA GTX 580 and 2 NVIDIA GTX 680 GPU cluster engineered by Accelera.<sup>35</sup> In the following, the numbering of the amino acids follows the arbitrary scheme by Ballesteros and Weinstein: each amino acid identifier starts with the helix number, followed by the position relative to a reference residue among the most conserved amino acids in that helix, to which the number 50 is arbitrarily assigned.<sup>36</sup>

**Homology Models.** The selected five crystal structures (PDB IDs: 3EML, 3UZA, 3UZC, 3RFM, and 2YDV) and the FASTA sequence of the hA<sub>2A</sub> AR (Uniprot ID: P29274) were retrieved from the RCSB PDB database<sup>37</sup> (<http://www.rcsb.org>) and the UniProtKB/Swiss-Prot,<sup>38–40</sup> respectively. As missing loop portions and replacement of the third intracellular loop with fusion proteins remarkably compromise the stability of the receptor as well as its flexibility during the MD simulations, for our study we employed homology models build upon the corresponding crystal structure. Therefore, eventual lysozyme portion fused to the receptor as well as cocrystallized ligands and water molecules have been removed before starting the homology modeling procedure. Ionization states and hydrogen positions have been assigned with the “Protonate-3D” tools.<sup>41</sup> Then, to minimize contacts among hydrogen atoms, the structures were subjected to energy minimization with Amber99 force field<sup>42</sup> until the root mean square (rms) of

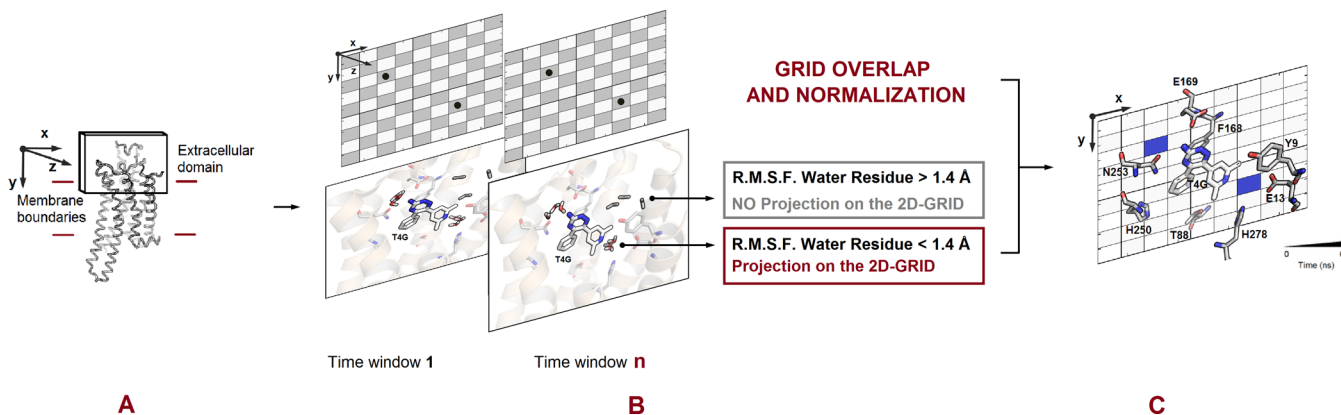


**Figure 1.** Workflow of the water fluid dynamics (WFD) maps construction process. Panel A: 3D-BOX definition that circumscribes the orthosteric binding site; panel B: 2D-GRID projection of water molecules that get geometrically trapped during MD simulations; panel C: 2D-GRIDS overlap and WFD simplified representation.

conjugate gradient was  $<0.05 \text{ kcal}\cdot\text{mol}^{-1}\cdot\text{\AA}^{-1}$ , by keeping the heavy atoms fixed at their crystallographic positions. The FASTA sequence was aligned, using Blosum 62 matrix, with the template sequence. Backbone and conserved residues coordinates were copied from the template structure, whereas newly modeled regions and nonconserved residues side chains were modeled and energetically optimized by using Amber99 force field until a rms of conjugate gradient  $<0.05 \text{ kcal}\cdot\text{mol}^{-1}\cdot\text{\AA}^{-1}$  was reached. Missing loop domains were constructed by the loop search method implemented in Molecular Operating Environment<sup>43</sup> (MOE, version 2012.10) on the basis of the structure of compatible fragments found in the Protein Data Bank.<sup>37</sup> N-terminal and C-terminal were deleted if their lengths exceeded those found in the crystallographic template. The “Protonate-3D” tool<sup>41</sup> was used to appropriately assign ionization states and hydrogen positions to the build models. Protein stereochemistry evaluation was then performed by employing several tools (Ramachandran and  $\chi$  plots measure  $\text{j}/\psi$  and  $\chi_1/\chi_2$  angles, clash contacts reports) implemented in the MOE suite.

**Molecular Dynamics.** Each ligand–receptor complex was embedded in a 1-palmitoyl-2-oleoyl-*sn*-glycero-3-phosphocholine (POPC) lipid bilayer ( $75 \times 75 \text{ \AA}$  wide) and placed into the membrane according to the suggested orientation reported in the “Orientations of Proteins in Membranes (OPM)” database<sup>44</sup> for the hA<sub>2A</sub> AR in complex with the antagonist T4G (PDB ID: 3UZA<sup>33</sup>). Ligand–receptor complexes, where the crystal structure was not available, were obtained by molecular docking using the protocol previously described<sup>45</sup> and physical-chemical descriptors, reported in Table 1, were calculated using MOE Suite. Overlapping lipids (within  $0.6 \text{ \AA}$ ) were removed upon insertion of the protein. The prepared systems were solvated with TIP3P<sup>46</sup> water using the program Solvate 1.0<sup>47</sup> and neutralized by Na<sup>+</sup>/Cl<sup>-</sup> counterions to a final concentration of 0.154 M. The total number of atoms per system was approximately 75 000. Membrane MD simulations were carried out on a GPU cluster with the ACEMD program<sup>48</sup> using the CHARMM27 Force Field<sup>49</sup> and periodic boundaries conditions. Initial parameters for the ligands were derived from the CHARMM General Force Field for organic molecules<sup>50</sup> by using the “paramchem” service<sup>51,52</sup> and were subsequently optimized at the MP2/6-31G\* level of theory<sup>53</sup> (consistently with the CHARMM27 Force Field parametrization) by using Gaussian 09<sup>54</sup> and the implemented parametrization tools in the VMD engine.<sup>55</sup>

The system was equilibrated using a stepwise procedure. In the first stage, to reduce steric clashes due to the manual setting up of the membrane-receptor system, a 500 steps conjugate-gradient minimization was performed. Then, to allow lipids to reach equilibrium and water molecules to diffuse into the protein cavity, the system was equilibrated by keeping the positions of protein and ligand atoms restrained for the first 8 ns by a force constant of  $1 \text{ kcal/mol}\cdot\text{\AA}^2$  and then by keeping only the  $\alpha$  carbon atoms frozen up to 9 ns while gradually reducing the force constant to  $0.1 \text{ kcal/mol}\cdot\text{\AA}^2$ . During the equilibration procedure, the temperature was maintained at 298 K using a Langevin thermostat with a low damping constant of  $1 \text{ ps}^{-1}$ , and the pressure was maintained at 1 atm using a Berendsen barostat. Bond lengths involving hydrogen atoms were constrained using the M-SHAKE<sup>56</sup> algorithm with an integration time step of 2 fs. Harmonical constraints were then removed during additional 60 ns (NVT ensemble). Long-range Coulomb interactions were handled using the particle mesh Ewald summation method (PME)<sup>57</sup> with grid size rounded to the approximate integer value of cell wall dimensions. A nonbonded cutoff distance of  $9 \text{ \AA}$  with a switching distance of  $7.5 \text{ \AA}$  was used.

**Water Fluid Dynamics (WFD) Maps.** Trajectory analysis, water clustering and water fluid dynamics (WFD) maps have been generated following the scheme reported in Figure 1 by using several functionalities implemented in VMD,<sup>55</sup> WOR-DOM,<sup>58</sup> PyMOL,<sup>59</sup> Gnuplot,<sup>60</sup> and Gromacs tools.<sup>61</sup> For the construction of WFD maps from the native MD trajectories the following procedure has been followed:

- The orthosteric binding site has been defined by selecting residues within a range of  $5 \text{ \AA}$  from the bound ligand (including E169[EL2], F168[EL2], His250[6.52], Asn253[6.55], T88[3.36], H278[7.43], E13[1.39], and Y9[1.35]), and a 3D BOX that circumscribes the binding site (Figure 1, panel A) has been created. The generated selection has been used to define the 3D BOX during the post processing of apoprotein MD trajectories.
- The built box has been split into a 3D-GRID to allow the monitoring of water molecules diffusion during the MD simulation and to localize specific grid cells where water molecules get trapped. Such GRID has been oriented parallel to the  $z$  axis (Figure 1, panel A) in order to make possible further projections of data on the  $xy$  plane.

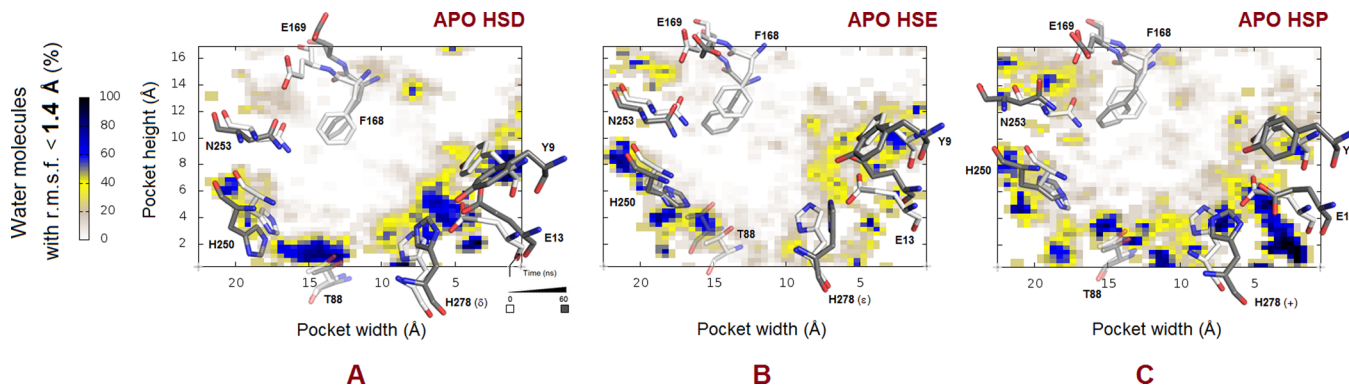


**Figure 2.** Probing His278 [7.43] tautomers effect on the hydro-dynamic profile of the apo-state of hA<sub>2A</sub> AR. Panel A:  $\delta$ -tautomer (HSD); panel B:  $\epsilon$ -tautomer (HSE); panel C: fully protonated state (HSP). Region colored in white-light green define bulk water occupancy. Yellow-blue areas define protein “hot-spots” where transient water molecules get trapped during MD simulations. Receptors are viewed from the membrane side facing TM6 and TM7. Conformations of side chains of the amino acids crucial for ligand binding are displayed as white and gray sticks at the start and the end of MD simulations, respectively. Hydrogen atoms are not displayed.

- Each MD trajectory has been split in regular time windows of 200 ps in accordance to previous studies on protein hydration.<sup>62</sup> Snapshots of the system coordinates have been saved every 10 ps. Each set of frames has been processed by calculating the root-mean-square fluctuation (rmsf) of all water molecules contained in the region defined by the originally created box. In particular (see Figure 1, panel B):
  - If the rmsf of a specific water molecule is below 1.4 Å, its position is averaged and projected on the *xy* plane. Averaged coordinates of projected water molecules have been recorded into a cumulative PDB file.
  - Otherwise, if the rmsf is above 1.4 Å, no projection on the 2D-GRID is made.
- Resulting 2D-GRIDs are overlapped and grid cells color-coded by normalizing the residence time of water molecules on a scale from 0% to 100% (Figure 1, panel C): In particular, white zones (0%) correspond to regions where water molecules have a residence time equivalent to bulk water and their position cannot be univocally determined, whereas blue regions (100%) correspond to where water molecules get trapped, have the maximum residence time of the considered trajectory frame, and which position could be determined with certainty ( $\text{rmsf} < 1.4 \text{ \AA}$ ).

The maps allow a fast graphical identification of structural and bulk water distribution inside the hA<sub>2A</sub> AR orthosteric binding pocket. Therefore, the hereby described protocol might help in predicting regions where water molecules can be found in 3D structures, in case a crystal structure is not yet available or has not been solved at high resolution.

## RESULTS AND DISCUSSION

**General Features of the Orthosteric Binding Site of the hA<sub>2A</sub> AR.** The binding site of the hA<sub>2A</sub> AR has been exhaustively described elsewhere.<sup>63</sup> We therefore report here the most relevant receptor–ligand binding features that describe the common interaction pattern for AR ligands, which are depicted in Figure S1 in Supporting Information. This analysis has been carried out by visually inspecting the crystallographic structures of hA<sub>2A</sub> AR that have been solved and published. The aromatic scaffold of agonists or antagonists

is involved an aromatic  $\pi$ – $\pi$  stacking with the conserved Phe168, located in the second extracellular loop [EL2], and additional hydrophobic contacts with, among others, the Leu249 [6.51] side chain. Strong polar interactions are established with the side chain of the conserved Asn253 [6.55],<sup>64</sup> where the role of the hydrogen bond donor in the high-affinity ligands is played, in most cases, by an exocyclic amino group. Moreover, in the agonist-bound crystal structure the Thr88 [3.36] side chain forms a hydrogen bond interaction with the nitrogen atom of the acetamide moiety in NECA. This pattern is consistent with the previously reported mutation data, which have been recently reviewed,<sup>65</sup> showing loss of affinity for the Asn253 [6.55] mutant, as well as with recent mutagenesis data revealing the critical role of Phe168 [EL2] and Leu249 [6.51] for both agonists and antagonists binding and of Thr88 [3.36] for agonist binding.<sup>65</sup>

Recent advances in structural biology have allowed investigators to crystallize and resolve a high-resolution structure of the A<sub>2A</sub> AR,<sup>29</sup> thus describing how water molecules play a crucial role in bridging protein–ligand interactions by forming a network of hydrogen bonding interaction between Tyr9 [1.35] Glu13 [1.39] and His278 [7.43] and the antagonist ZM 241385. Such piece of information, however, is still missing for other potent hA<sub>2A</sub> AR antagonists that belong to chemical classes that possess more favorable ADME properties.

**Exploring WFD Map of the hA<sub>2A</sub> AR Apo-State.** The structure of the hA<sub>2A</sub> AR in its apo-state has not been solved yet. In order to depict the possible dynamic organization of water molecules inside the orthosteric binding cleft, the apo-form of the receptor has been embedded in a POPC lipid bilayer and water fluid dynamics (WFD) maps have been generated (Figure 2). The WFD maps highlight the propensity of specific region of the orthosteric site, namely, hot-spots, to trap water molecules as suggested by their residence time (Figure 2A–C): water molecules in proximity of Tyr9 [1.35], Glu13 [1.39], Thr88 [3.36], His250 [6.52] are characterized by an  $\text{rmsf} < 1.4 \text{ \AA}$ , over 200 ps, hence suggesting a crucial role in defining the topological and interactive properties of the portion of the orthosteric site. Interestingly, these residues are conserved in all cloned adenosine receptors,<sup>66</sup> and their involvement in the ligand binding process has been demonstrated.<sup>66–70</sup> In particular, Glu13 [1.39] and His278 [7.43] have been shown to play a critical role in agonist<sup>71</sup> and antagonist recognition and in the allosteric regulation mediated

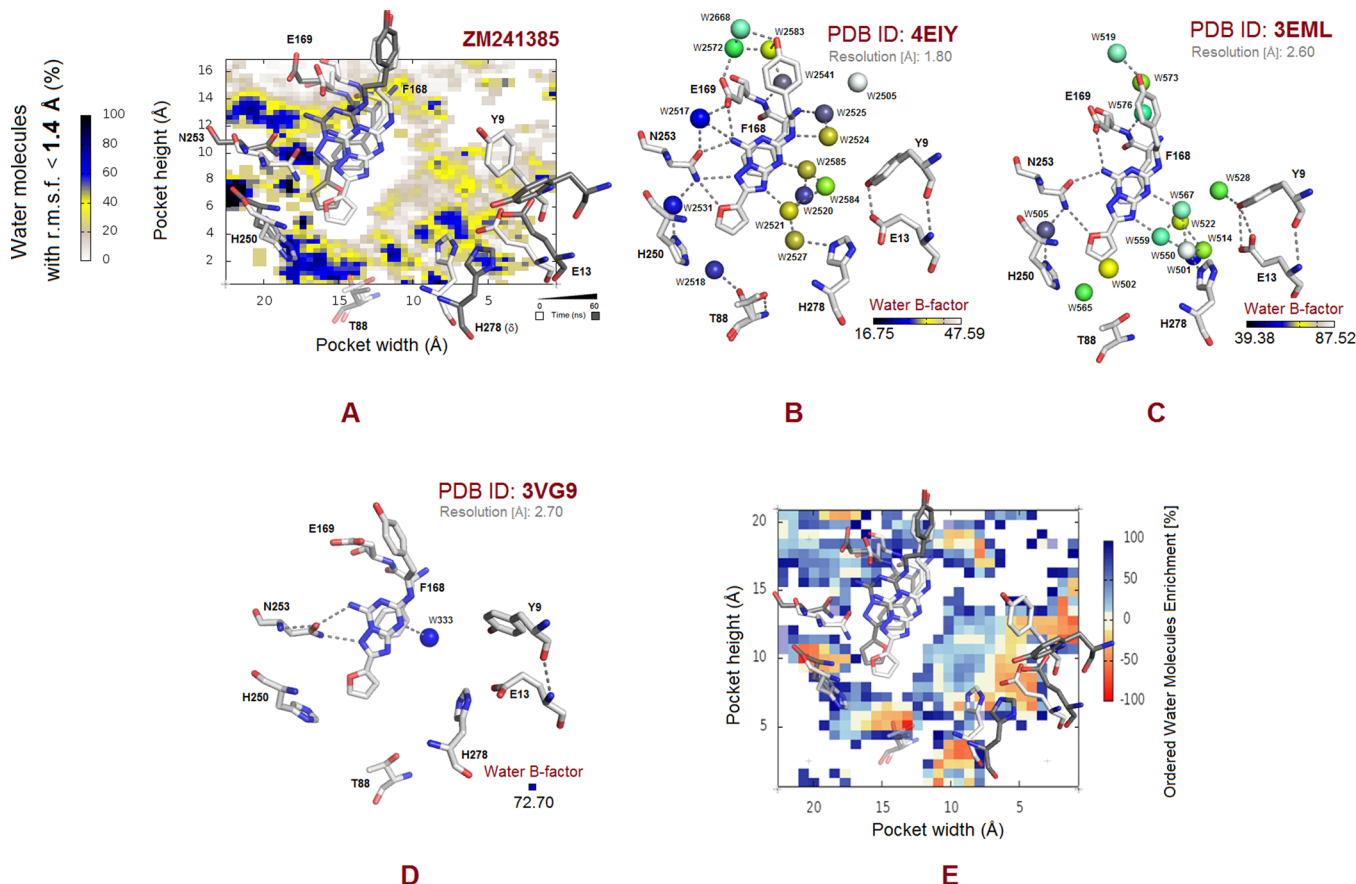


**Figure 3.** WFD map for ZM 241385-hA<sub>2A</sub> AR complex (panel A); panels B,C,D: position of water molecules experimentally determined in high resolution X-ray structures; panel E: ordered water molecules enrichment in comparison to the apo-state of hA<sub>2A</sub> AR. Receptors are viewed from the membrane side facing TM6 and TM7. Conformations of side chains of the amino acids crucial for ligand binding are displayed as white and gray sticks at the start and the end of MD simulations, respectively. Hydrogen atoms are not displayed.

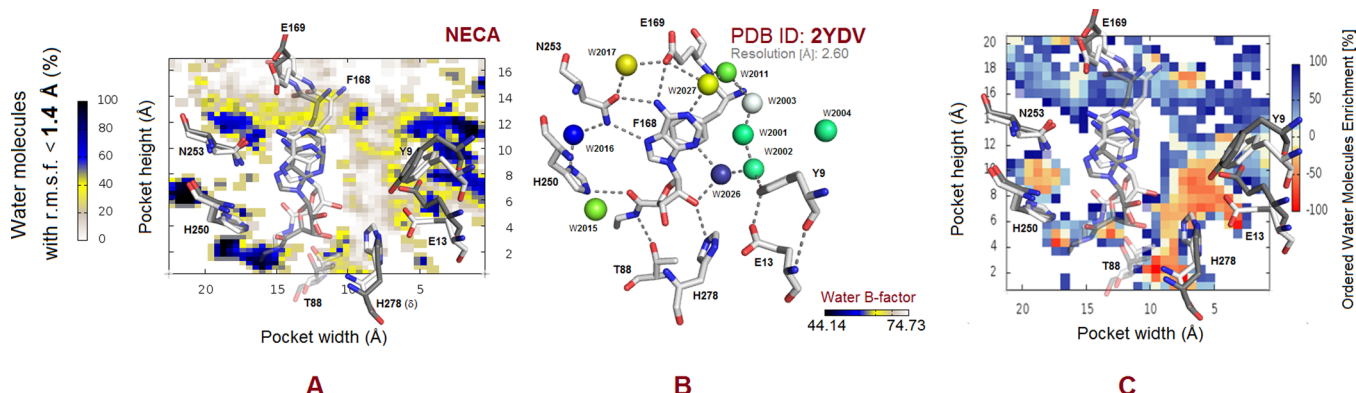


**Figure 4.** WFD map for NECA-hA<sub>2A</sub> AR complex (panel A); panel B: position of water molecules experimentally determined in high resolution X-ray structures; panel C: ordered water molecules enrichment in comparison to the apo-state of hA<sub>2A</sub> AR. Receptors are viewed from the membrane side facing TM6 and TM7. Conformations of side chains of the amino acids crucial for ligand binding are displayed as white and gray sticks at the start and the end of MD simulations, respectively. Hydrogen atoms are not displayed.

by sodium ions.<sup>29</sup> Concerning His 278 [7.43], our data suggest that the  $\epsilon$ -tautomer (HSE, Figure 2B) has much less propensity to coordinate water molecules as compared to its  $\delta$ -tautomer (HSD, Figure 2A) and protonated state (HSP, Figure 2C). The other water molecules not directly interacting with the aforementioned residues have a residence time comparable to the water in the bulk liquid. These molecules are more likely to be replaced upon ligand binding at no energetic cost.

**Exploring Ligand-Bound hA<sub>2A</sub> AR WFD Maps.** The WFD maps corresponding to the ZM 241385-hA<sub>2A</sub> AR complex (Figure 3A) highlight the presence of an enriched arrangement of water molecules that bridges Tyr9 [1.35], Glu13 [1.39], and His278 [7.43] to the triazolotriazine core of the antagonist as compared to the WFD map of the apo-state of the receptor. Additionally, the hot-spots located in the proximity of Asn253 [6.55] and Glu169 [EL2] reveal that the interactions that those residues establish with the exocyclic

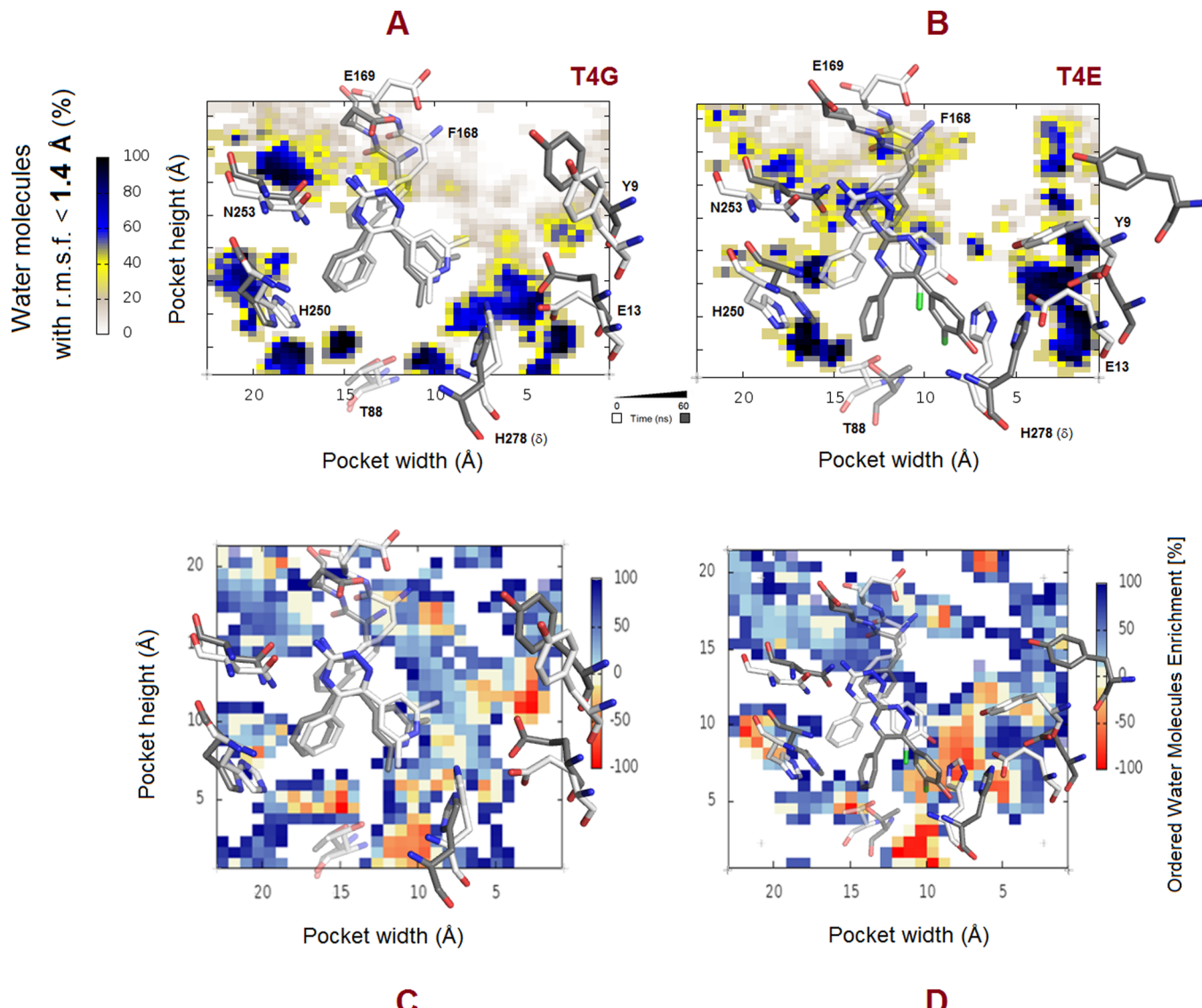


**Figure 5.** WFD maps map for T4G-hA<sub>2A</sub> AR complex (panel A) and T4E-hA<sub>2A</sub> AR (panel B). Panel C,D: ordered water molecules enrichment in comparison between the apo-state of hA<sub>2A</sub> AR and WFD of hA<sub>2A</sub> AR bound-T4G and T4E, respectively. Receptors are viewed from the membrane side facing TM6 and TM7. Conformations of side chains of the amino acids crucial for ligand binding are displayed as white and gray sticks at the start and the end of MD simulations. Hydrogen atoms are not displayed.

nitrogen of the antagonist are stabilized by a cluster of water molecules. There is an excellent correlation with the experimental data (Figure 3B): In fact, the WFD map resulting from our analysis reflects the arrangement and B-factor of water molecules in the crystal structure (PDB ID: 4EIY<sup>30</sup>). Water molecules W2527, W2521, W2520, W2584, W2585, W2524, and W2525 in the X-RAY structure interact with the triazolotriazine core of the antagonist and Tyr9 [1.35], Glu13 [1.39], and His278 [7.43] and are located in geometrical positions were structural water molecules have been predicted to be by our WFD map (Figure 3A). Water W2517 interacts with Asn253 [6.55], Glu169 [EL2] and the exocyclic nitrogen of ZM 241385. Water W2572, W2668, W2583, and W2541 surround the phenol moiety of the antagonist and Glu169 [EL2]. Temperature factor values of water molecules that surround the antagonist in the crystallographic structure range from 16.75 to 47.59: To better show the convergence of our results with the experimental data, in Figure 3B–D, the molecules have been colored following the same color code

used to generate the WFD maps. As can be noted, the correspondence of the relative vibrational motion to the reduced ability to fluctuate over time calculated on MD trajectories is straightforward. Lower-resolution crystal structures of hA<sub>2A</sub> AR in complex with the antagonist ZM241385 (PDB ID: 3EML<sup>32</sup> – Figure 3C; PDB ID: 3VG9<sup>72</sup> – Figure 3D) reveal a similar solvation pattern but with fewer details. As expected, ZM 241385 binding also induces a rearrangement of water molecules: In particular, upon ligand binding, water molecules that are bound to Thr 88 [3.36] side chains are displaced (as depicted in the map in Figure 3E representing by a color code the enrichment or displacement of water molecules as emerged by the comparison of the WFD maps of the apo and ligand-bound form).

In the agonist bound (NECA) hA<sub>2A</sub> AR complex the WFD map (Figure 4A) is highly correlated with the position and B-factor values of cocrystallized water molecules (PDB ID: 2YDV<sup>17</sup>). Water molecules W2017 and W2027 (Figure 4B) bridge the exocyclic nitrogen of the adenine ring to the Glu169

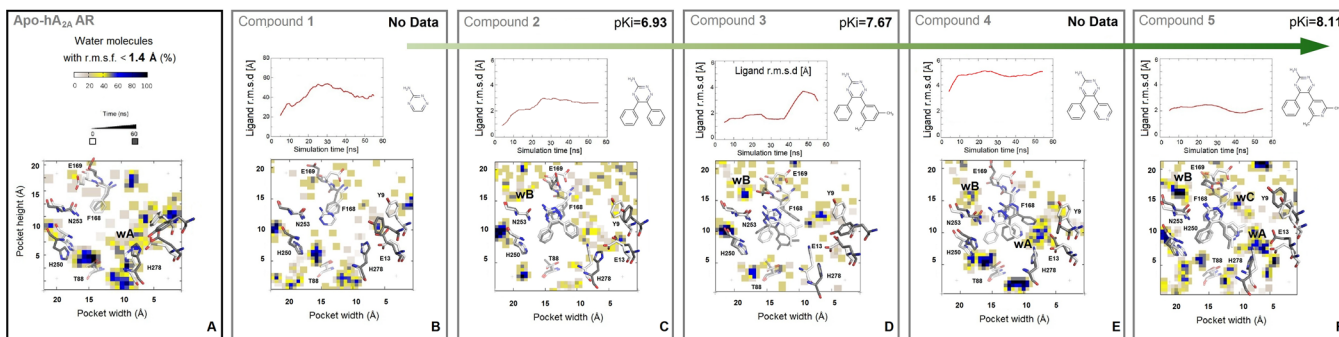


**Figure 6.** Panel A: hydro-dynamic profile of the apo-state of hA<sub>2A</sub> AR. Panels B–F: combined WFD maps and rmsd profiles for compound 1 to compound 5 into the hA<sub>2A</sub> AR binding pocket. Receptors are viewed from the membrane side facing TM6 and TM7. Conformations of side chains of the amino acids crucial for ligand binding are displayed as white and gray sticks at the start and the end of MD simulations, respectively. Hydrogen atoms are not displayed.

[EL2] and Asn253 [6.55] side chains and the arrangement of water molecules that surrounds Thr88 [3.36] and His278 [7.43] in the apo-state of hA<sub>2A</sub> AR are displaced by the direct interaction of the acetamide moiety of NECA with the hydroxyl group of side chain (Figure 4C). As reported for the antagonist ZM241385, Tyr9 [1.35] and Glu13 [1.39] represent hotspots that bridge TM1 to the aromatic scaffold of NECA through water molecules W2026, W2002, and W2001.

The binding modes of some potent 1,2,4-triazine derivatives, antagonist at the hA<sub>2A</sub> AR, have been revealed by X-ray crystallography,<sup>33</sup> and information about the role of water molecules in the binding has been recently investigated.<sup>30</sup> WFD maps obtained in this study (Figure 5A,B) are in agreement with previously reported data<sup>30</sup> and highlight that strong interactions between the Asn253 [6.55] and Glu169 [EL2] side chains and that the exocyclic nitrogen bound the 1,2,4-triazine core is stabilized by ordered water molecules. The nitrogen atom of the pyridyl moiety in T4G interacts with His278 [7.43] by an ordered cluster of water molecules (Figure 5A) and induces a rearrangement of water molecules that are bound to the Thr88 [3.36] side chain (Figure 5B). Upon the binding of the chloro-phenol derivative T4E (Figure 5C), the ordered cluster of water molecules bound to His278 [7.43] and Glu13 [1.39] are released into the bulk solvent (Figure 5D).

**WFD Maps as Supporting Tool for an Effective in Silico Drug Discovery Strategy.** As anticipated in the Introduction section, we investigated the time-dependent organization of water clusters within the orthosteric binding pocket of the apo-state of the hA<sub>2A</sub> AR and its ligand-bound state, focusing on various structurally related 1,2,4-triazine derivatives (Table 1) obtained by virtual modifications of the T4E structure. Compound 1 (Table 1) is predicted to be the most polar of the considered set of molecules and is characterized by a small van der Waals volume (115.50 Å<sup>3</sup>). There is no proven binding of this molecules to the human A<sub>2A</sub> AR and the MD simulation reveal the unbinding (root mean square deviation, rmsd > 20 Å) of the originally docked compound from the orthosteric binding pocket. The analysis of the WFD map of the orthosteric binding pocket (Figure 6B) suggest that ligand-binding would involve a loss of water molecules (wA cluster, Figure 6A) that are bound to specific hotspots of the receptor such as the triad Tyr9 [1.35], Glu13 [1.39], and His278 [7.43]. Such water molecules indeed would preferentially solvate the polar fragment-like molecule, thus facilitating its unbinding from the receptor.

The introduction of two phenyl groups in C5 and C6 of the triazine core considerably increases the volume of the derivative to 345.45 Å<sup>3</sup>, leading to the commercially available diphenyl-1,2,4-triazine-3-ammine (compound 2, Table 1). The phenyl substituent attached to the C5 position occupies the hydrophobic pocket enclosed by Leu84 [3.32], Leu85 [3.33], Met177 [5.38], Trp246 [6.48], Leu249 [6.51], and His250 [6.52] (data not shown). The phenyl substituent attached to C6 points toward a hydrophobic region defined by Ala63 [2.61] and Ile66 [2.64], and the His278 [7.43]. The chemical modification that leads to the dimethyl-phenyl derivative (compound 3, Table 1) provides enhanced surface complementarity between ligand and receptor, thus potentially improving ligand binding. The corresponding WDF maps show that, upon ligand binding, a cluster of water molecules (wB cluster, Figure 6C,D) mediates the interactions between Glu169 [EL2], Asn253 [6.55], and the exocyclic nitrogen bound to the triazine ring.

Interestingly, the hydrophobic moieties of compounds 2 and 3 that point toward Tyr9 [1.35], Glu13 [1.39] and His278 [7.43] unhinge the water molecules network that is present in the neighboring region prior ligand binding. These results are in agreement with the prediction of “unhappy” water molecules in the proximity of His250 [6.52] and His278 [7.43], and the short residence time that have been recently reported for these virtual compounds.<sup>30</sup>

The insertion of a pyridyl substituent at the C6 position of the triazine ring (compound 4, Table 1) results in the creation of two structural water molecules arrangements (wA and wB clusters, Figure 6E), that mediate the interactions between Glu169 [EL2], Asn253 [6.55] and the exocyclic nitrogen bound to the triazine ring and bridge the pyridyl nitrogen to Glu13 [1.39] and His278 [7.43].

The combination of the modifications that lead from compound 2 to the compound 5 (Table 1)—i.e., the 3–5-methylation and the insertion of a nitrogen atom in the para position of the substituent attached to the C6 position of the triazine ring—increased affinity to the hA<sub>2A</sub> AR of about an order of magnitude. Our WFD map suggest that such increase in the binding affinity might be due to the peculiar arrangement of water molecules around the ligand are characterized by low fluctuation during MD simulations.

The three stable clusters of water molecules, namely, wA, wB and wC, emerged by our WFD maps (Figure 6F) are found to interact with both the receptor and the ligand, thus contributing to its low fluctuation inside the orthosteric binding site (rmsd < 2.5 Å) and might provide a rationale for the slower off-rate

receptor kinetics ( $\sim 2$  orders of magnitude)<sup>30</sup> of compound 5 ( $1.15 \times 10^{-2}$ ) with respect to the other derivatives.

## CONCLUSIONS

We have presented here an alternative approach to identify protein “hot-spots”, that is, water molecules characterized by peculiar shape and electrostatic properties that can play critical role in ligand binding. The proposed methodology inspects the variation of fluid dynamics properties of water molecules upon ligand binding by monitoring the time-dependent organization of water molecules during the final stage of the ligand–receptor recognition process. Through a postprocessing analysis of MD trajectories, our approach returns bidimensional graphs that we called water fluid dynamics (WFD) maps that allow a fast graphical identification of protein “hot-spots”. Interestingly, our methodology can be applied with any simulation package that can be engineered to run on GPUs.

From a medicinal chemistry point of view, the generated WFD maps and 3D structure files (see Supporting Information) can be used in tandem with other approaches to carry out intelligent scaffold replacement, or other chemical modifications, that do not displace crucial water molecules, thus potentially ensuring the desired potency and selectivity profile. This approach could simplify the discovery of a new nonfuran, nonxanthine, and relatively polar hA<sub>2A</sub> AR targeting agent characterized with an eased path to approval. Moreover, we believe that the proposed approach can be extended also to other GPCRs as well as to homology models.

## ASSOCIATED CONTENT

### Supporting Information

WFD map of the caffeine-hA<sub>2A</sub> AR recognition is reported in Figure S2 in the Supporting Information material. PDB files of the apo-state of hA2A AR in three His278 [7.43] tautomeric/protomeric situations ( $\delta$ -tautomer: APO\_H278\_HSD.pdb;  $\epsilon$ -tautomer: APO\_H278\_HSE.pdb; fully protonated state: APO\_H278\_HSP.pdb) including highly residential water molecules. This material is available free of charge via the Internet at <http://pubs.acs.org>

## AUTHOR INFORMATION

### Corresponding Author

\*E-mail: stefano.moro@unipd.it. Fax: +39 049 827 5366. Tel.: +39 049 8275704.

### Notes

The authors declare no competing financial interest.

## ACKNOWLEDGMENTS

The molecular modeling work coordinated by S.M. has been carried out with financial support of the University of Padova, Italy, and the Italian Ministry for University and Research (MIUR), Rome, Italy. S.M. is also very grateful to Chemical Computing Group and Accellera Ltd. for the scientific and technical partnership. S.M. participates in the European COST Action CM1207 (GLISTEN)

## ABBREVIATIONS:

ARs, Adenosine Receptors; EL2, Second Extracellular Loop; GPCRs, G Protein-Coupled Receptors; GPU, Graphics Processing Unit; WFD maps, Water Fluid Dynamics maps; MD, Molecular Dynamics; n.d., not determined; NECA, N-Ethyl-5'-Carboxamido Adenosine; POPC, 1-Palmitoyl-2-oleoyl-

*sn*-glycero-3-phosphocholine; T4E, 4-(3-Amino-5-phenyl-1,2,4-triazin-6-yl)-2-chlorophenol; T4G, 6-(2,6-Dimethylpyridin-4-yl)-5-phenyl-1,2,4-triazin-3-amine; TM, Transmembrane; ZM 241385, 4-(2-(7-Amino-2-(2-furyl)(1,2,4)triazolo(2,3-a)-(1,3,5)triazin-5-yl-amino)ethyl)phenol

## REFERENCES

- (1) Ball, P. Water as an Active Constituent in Cell Biology. *Chem. Rev.* **2008**, *108*, 74–108.
- (2) Lemieux, R. U. How Water Provides the Impetus for Molecular Recognition in Aqueous Solution. *Acc. Chem. Res.* **1996**, *29*, 373–380.
- (3) Babine, R. E.; Bender, S. L. Molecular Recognition of Protein-Ligand Complexes: Applications to Drug Design. *Chem. Rev.* **1997**, *97*, 1359–1472.
- (4) Cappel, D.; Wahlstrom, R.; Brenk, R.; Sotriffer, C. A. Probing the Dynamic Nature of Water Molecules and their Influences on Ligand Binding in a Model Binding Site. *J. Chem. Inf. Model.* **2011**, *51*, 2581–2594.
- (5) Cheng, T.; Li, Q.; Zhou, Z.; Wang, Y.; Bryant, S. H. Structure-based Virtual Screening for Drug Discovery: a Problem-centric Review. *AAPS J.* **2012**, *14*, 131–141.
- (6) Wong, S. E.; Lightstone, F. C. Accounting for Water Molecules in Drug Design. *Expert Opin. Drug Discovery* **2011**, *6*, 65–74.
- (7) Huggins, D. J.; Tidor, B. Systematic Placement of Structural Water Molecules for Improved Scoring of Protein-Ligand Interactions. *Prot. Eng. Des. Sel.* **2011**, *24*, 777–789.
- (8) Lu, Y. P.; Wang, R. X.; Yang, C. Y.; Wang, S. M. Analysis of Ligand-Bound Water Molecules in High-Resolution Crystal Structures of Protein-Ligand Complexes. *J. Chem. Inf. Model.* **2007**, *47*, 668–675.
- (9) Snyder, P. W.; Mecinović, J.; Moustakas, D. T.; Thomas, S. W.; Harder, M.; Mack, E. T.; Lockett, M. R.; Héroux, A.; Sherman, W.; Whitesides, G. M. Mechanism of the Hydrophobic Effect in the Biomolecular Recognition of Arylsulfonamides by Carbonic Anhydrase. *Proc. Natl. Acad. Sci. U.S.A.* **2011**, *108*, 17889–17894.
- (10) De Lucca, G. V.; Erickson-Viitanen, S.; Lam, P. Y. S. Cyclic HIV Protease Inhibitors Capable of Displacing the Active Site Structural Water Molecule. *Drug Discovery Today* **1997**, *2*, 6–18.
- (11) De Beer, S. B. A.; Vermeulen, N. P. E.; Oostenbrink, C. The Role of Water Molecules in Computational Drug Design. *Curr. Top. Med. Chem.* **2010**, *10*, 55–66.
- (12) Carugo, O.; Bordo, D. How Many Water Molecules can be Detected by Protein Crystallography? *Acta Crystallogr., Sect. D: Biol. Crystallogr.* **1999**, *55*, 479–483.
- (13) Goodford, P. J. A Computational Procedure for Determining Energetically Favorable Binding Sites on Biologically Important Macromolecules. *J. Med. Chem.* **1985**, *28*, 849–857.
- (14) Pitt, W. R.; Goodfellow, J. M. Modelling of Solvent Positions around Polar Groups in Proteins. *Protein Eng.* **1991**, *4*, 531–537.
- (15) Verdonk, M. L.; Cole, J. C.; Taylor, R. SuperStar: a Knowledge-Based Approach for Identifying Interaction Sites in Proteins. *J. Mol. Biol.* **1999**, *289*, 1093–1108.
- (16) Rossato, G.; Ernst, B.; Vedani, A.; Smiesko, M. AcquaAlta: a Directional Approach to the Solvation of Ligand-Protein Complexes. *J. Chem. Inf. Model.* **2011**, *51*, 1867–1881.
- (17) Kellogg, G. E.; Chen, D. L. The Importance of Being Exhaustive. Optimization of Bridging Structural Water Molecules and Water Networks in Models of Biological Systems. *Chem. Biodiversity* **2004**, *1*, 98–105.
- (18) Ross, G. A.; Morris, G. M.; Biggin, P. C. Rapid and Accurate Prediction and Scoring of Water Molecules in Protein Binding Sites. *PLoS One* **2012**, *7*, e32036.
- (19) Imai, T.; Hiraoka, R.; Kovalenko, A.; Hirata, F. Locating Missing Water Molecules in Protein Cavities by the Three-Dimensional Reference Interaction Site Model Theory of Molecular Solvation. *Proteins* **2007**, *66*, 804–813.
- (20) Barillari, C.; Taylor, J.; Viner, R.; Essex, J. W. Classification of water molecules in protein binding sites. *J. Am. Chem. Soc.* **2007**, *129*, 2577–2587.

- (21) Michel, J.; Tirado-Rives, J.; Jorgensen, W. L. Energetics of Displacing Water Molecules from Protein Binding Sites: Consequences for Ligand Optimization. *J. Am. Chem. Soc.* **2009**, *131*, 15403–15411.
- (22) Li, Z.; Lazaridis, T. Thermodynamics of Buried Water Clusters at a Protein-Ligand Binding Interface. *J. Phys. Chem. B* **2006**, *110*, 1464–1475.
- (23) Young, T.; Abel, R.; Kim, B.; Berne, B. J.; Friesner, R. A. Motifs for Molecular Recognition Exploiting Hydrophobic Enclosure in Protein-Ligand Binding. *Proc. Natl. Acad. Sci. U.S.A.* **2007**, *104*, 808–813.
- (24) Lingle Wang, L.; Berne, B. J.; Friesner, R. A. Ligand Binding to Protein-Binding Pockets with Wet and Dry Regions. *Proc. Natl. Acad. Sci. U.S.A.* **2011**, *108*, 1326–1330.
- (25) Huggins, D. J.; Marsh, M.; Payne, M. C. Thermodynamic Properties of Water Molecules at a Protein Protein Interaction Surface. *J. Chem. Theory Comput.* **2011**, *7*, 3514–3522.
- (26) Pardo, L.; Deupi, X.; Döller, N.; López-Rodríguez, M. L.; Campillo, M. The Role of Internal Water Molecules in the Structure and Function of the Rhodopsin Family of G Protein-Coupled Receptors. *ChemBioChem* **2007**, *8*, 19–24.
- (27) Angel, T. E.; Gupta, S.; Jastrzebska, B.; Palczewski, K.; Chance, M. R. Structural Waters Define a Functional Channel Mediating Activation of the GPCR, Rhodopsin. *Proc. Natl. Acad. Sci. U.S.A.* **2009**, *106*, 14367–14372.
- (28) Jastrzebska, B.; Palczewski, K.; Golczak, M. Role of Bulk Water in Hydrolysis of the Rhodopsin Chromophore. *J. Biol. Chem.* **2011**, *286*, 18930–18937.
- (29) Liu, W.; Chun, E.; Thompson, A. A.; Chubukov, P.; Xu, F.; Katritch, V.; Han, G. W.; Roth, C. B.; Heitman, L. H.; Ijzerman, A. P.; Cherezov, V.; Stevens, R. C. Structural Basis for Allosteric Regulation of GPCRs by Sodium Ions. *Science* **2012**, *337*, 232–236.
- (30) Bortolato, A.; Tehan, B. G.; Bodnarchuk, M. S.; Essex, J. W.; Mason, J. S. Water Network Perturbation in Ligand Binding: Adenosine A2A Antagonists as a Case Study. *J. Chem. Inf. Model.* **2013**, *53*, 1700–1713.
- (31) Doré, A. S.; Robertson, N.; Errey, J. C.; Ng, I.; Hollenstein, K.; Tehan, B.; Hurrell, E.; Bennett, K.; Congreve, M.; Magnani, F.; Tate, C. G.; Weir, M.; Marshall, F. H. Structure of the Adenosine A(2A) Receptor in Complex with ZM241385 and the Xanthines XAC and Caffeine. *Structure* **2011**, *19*, 1283–1293.
- (32) Jaakola, V.-P.; Griffith, M. T.; Hanson, M. A.; Cherezov, V.; Chien, E. Y. T.; Lane, J. R.; Ijzerman, A. P.; Stevens, R. C. The 2.6 Ångstrom Crystal Structure of a Human A<sub>2A</sub> Adenosine Receptor Bound to an Antagonist. *Science* **2008**, *322*, 1211–1217.
- (33) Congreve, M.; Andrews, S. P.; Doré, A. S.; Hollenstein, K.; Hurrell, E.; Langmead, C. J.; Mason, J. S.; Ng, I. W.; Tehan, B.; Zhukov, A.; Weir, M.; Marshall, F. H. Discovery of 1,2,4-Triazine Derivatives as Adenosine A(2A) Antagonists using Structure Based Drug Design. *J. Med. Chem.* **2012**, *55*, 1898–1903.
- (34) Lebon, G.; Warne, T.; Edwards, P. C.; Bennett, K.; Langmead, C. J.; Leslie, A. G. W.; Tate, C. G. Agonist-bound Adenosine A<sub>2A</sub> Receptor Structures Reveal Common Features of GPCR Activation. *Nature* **2011**, *474*, 521–525.
- (35) AcCellera. <http://www.accellera.com/>.
- (36) Ballesteros, J. A.; Weinstein, H. Integrated Methods for the Construction of Three-Dimensional Models and Computational Probing of Structure-Function Relations in G Protein-Coupled Receptors. In *Methods in Neurosciences*; Sealfon, S. C., Ed.; Academic Press, 1995; Vol. 25, pp 366–428.
- (37) Berman, H. M.; Westbrook, J.; Feng, Z.; Gilliland, G.; Bhat, T. N.; Weissig, H.; Shindyalov, I. N.; Bourne, P. E. The Protein Data Bank. *Nucleic Acids Res.* **2000**, *28*, 235–242.
- (38) The EMBL Outstation, The European Bioinformatics Institute, Wellcome Trust Genome Campus, Hinxton, Cambridge. The Universal Protein Resource (UniProt) in 2010. *Nucleic Acids Res.* **2010**, *38*, D142–D148.
- (39) Jain, E.; Bairoch, A.; Duvaud, S.; Phan, L.; Redaschi, N.; Suzek, B. E.; Martin, M. J.; McGarvey, P.; Gasteiger, E. Infrastructure for the Life Sciences: Design and Implementation of the UniProt Website. *BMC Bioinf.* **2009**, *10*, 136.
- (40) Altschul, S. F.; Madden, T. L.; Schäffer, A. A.; Zhang, J.; Zhang, Z.; Miller, W.; Lipman, D. J. Gapped BLAST and PSI-BLAST: A New Generation of Protein Database Search Programs. *Nucleic Acids Res.* **1997**, *25*, 3389–3402.
- (41) Labute, P. Protonate3D: Assignment of Ionization States and Hydrogen Coordinates to Macromolecular Structures. *Proteins* **2009**, *75*, 187–205.
- (42) Wang, J.; Cieplak, P.; Kollman, P. A. How Well Does a Restrained Electrostatic Potential (RESP) Model Perform in Calculating Conformational Energies of Organic and Biological Molecules? *J. Comput. Chem.* **2000**, *21*, 1049–1074.
- (43) Molecular Operating Environment. <http://www.chemcomp.com/>.
- (44) Lomize, M. A.; Lomize, A. L.; Pogozheva, I. D.; Mosberg, H. I. OPM: Orientations of Proteins in Membranes Database. *Bioinformatics* **2006**, *22*, 623–625.
- (45) Inamdar, G. S.; Pandya, A. N.; Thakar, H. M.; Sudarsanam, V.; Kachler, S.; Sabbadini, D.; Moro, S.; Klotz, K.-N.; Vasu, K. K. New Insight into Adenosine Receptors Selectivity derived from a Novel Series of [5-substituted-4-phenyl-1,3-thiazol-2-yl] Benzamides and Furamides. *Eur. J. Med. Chem.* **2013**, *63*, 924–934.
- (46) Jorgensen, W. L.; Chandrasekhar, J.; Madura, J. D.; Impey, R. W.; Klein, M. L. Comparison of Simple Potential Functions for Simulating Liquid Water. *J. Chem. Phys.* **1983**, *79*, 926–935.
- (47) Helmut Grubmüller and Volker Groll Solvate. <http://www.mpibpc.mpg.de/home/grubmueller/downloads/solvate/index.html>.
- (48) Harvey, M. J.; Giupponi, G.; Fabritiis, G. D. ACEMD: Accelerating Biomolecular Dynamics in the Microsecond Time Scale. *J. Chem. Theory Comput.* **2009**, *5*, 1632–1639.
- (49) MacKerell, A. D., Jr; Banavali, N.; Foloppe, N. Development and Current Status of the CHARMM Force Field for Nucleic Acids. *Biopolymers* **2000**, *56*, 257–265.
- (50) Vanommeslaeghe, K.; Hatcher, E.; Acharya, C.; Kundu, S.; Zhong, S.; Shim, J.; Darian, E.; Guvench, O.; Lopes, P.; Vorobyov, I.; Mackerell, A. D., Jr CHARMM General Force Field: A Force Field for Drug-like Molecules Compatible with the CHARMM All-atom Additive Biological Force Fields. *J. Comput. Chem.* **2010**, *31*, 671–690.
- (51) Vanommeslaeghe, K.; MacKerell, A. D. Automation of the CHARMM General Force Field (CGenFF) I: Bond Perception and Atom Typing. *J. Chem. Inf. Model.* **2012**, *52*, 3144–3154.
- (52) Vanommeslaeghe, K.; Raman, E. P.; MacKerell, A. D. Automation of the CHARMM General Force Field (CGenFF) II: Assignment of Bonded Parameters and Partial Atomic Charges. *J. Chem. Inf. Model.* **2012**, *52*, 3155–3168.
- (53) Head-Gordon, M.; Pople, J. A.; Frisch, M. J. MP2 Energy Evaluation by Direct Methods. *Chem. Phys. Lett.* **1988**, *153*, 503–506.
- (54) Frisch, M. J.; Trucks, G. W.; Schlegel, H. B.; Scuseria, G. E.; Robb, M. A.; Cheeseman, J. R.; Scalmani, G.; Barone, V.; Mennucci, B.; Petersson, G. A.; Nakatsuji, H.; Caricato, M.; Li, X.; Hratchian, H. P.; Izmaylov, A. F.; Bloino, J.; Zheng, G.; Sonnenberg, J. L.; Hada, M.; Ehara, M.; Toyota, K.; Fukuda, R.; Hasegawa, J.; Ishida, M.; Nakajima, T.; Honda, Y.; Kitao, O.; Nakai, H.; Vreven, T.; Montgomery, J. A., Jr.; Peralta, J. E.; Ogliaro, F.; Bearpark, M.; Heyd, J. J.; Brothers, E.; Kudin, K. N.; Staroverov, V. N.; Kobayashi, R.; Normand, J.; Raghavachari, K.; Rendell, A.; Burant, J. C.; Iyengar, S. S.; Tomasi, J.; Cossi, M.; Rega, N.; Millam, M. J.; Klene, M.; Knox, J. E.; Cross, J. B.; Bakken, V.; Adamo, C.; Jaramillo, J.; Gomperts, R.; Stratmann, R. E.; Yazev, O.; Austin, A. J.; Cammi, R.; Pomelli, C.; Ochterski, J. W.; Martin, R. L.; Morokuma, K.; Zakrzewski, V. G.; Voth, G. A.; Salvador, P.; Dannenberg, J. J.; Dapprich, S.; Daniels, A. D.; Farkas, Ö.; Foresman, J. B.; Ortiz, J. V.; Cioslowski, J.; Fox, D. J. *Gaussian 09*, revision B.01; Gaussian, Inc.: Wallingford, CT, 2009.
- (55) Humphrey, W.; Dalke, A.; Schulten, K. VMD: Visual Molecular Dynamics. *J. Mol. Graph.* **1996**, *14*, 33–38.
- (56) Kräutler, V.; Van Gunsteren, W. F.; Hünenberger, P. H. A Fast SHAKE Algorithm to Solve Distance Constraint Equations for Small

Molecules in Molecular Dynamics Simulations. *J. Comput. Chem.* **2001**, *22*, 501–508.

(57) Essmann, U.; Perera, L.; Berkowitz, M. L.; Darden, T.; Lee, H.; Pedersen, L. G. A Smooth Particle Mesh Ewald Method. *J. Chem. Phys.* **1995**, *103*, 8577–8593.

(58) Seeber, M.; Felline, A.; Raimondi, F.; Muff, S.; Friedman, R.; Rao, F.; Caflisch, A.; Fanelli, F. Wordom: a User-Friendly Program for the Analysis of Molecular Structures, Trajectories, and Free Energy Surfaces. *J. Comput. Chem.* **2011**, *32*, 1183–1194.

(59) The PyMOL Molecular Graphics System, Version 1.5.0.4 Schrödinger, LLC.

(60) Williams, T. Kelley, C. Gnuplot: An Interactive Plotting Program; Available at: <http://www.gnuplot.info>.

(61) Van Der Spoel, D.; Lindahl, E.; Hess, B.; Groenhof, G.; Mark, A. E.; Berendsen, H. J. C. GROMACS: Fast, flexible, and free. *J. Comput. Chem.* **2005**, *26*, 1701–1718.

(62) Otting, G.; Liepinsh, E.; Wüthrich, K. Protein Hydration in Aqueous Solution. *Science* **1991**, *254*, 974–980.

(63) Jacobson, K. A.; Costanzi, S. New Insights for Drug Design from the X-ray Crystallographic Structures of G-Protein-Coupled Receptors. *Mol. Pharmacol.* **2012**, *82*, 361–371.

(64) Jaakola, V.-P.; Lane, J. R.; Lin, J. Y.; Katritch, V.; Ijzerman, A. P.; Stevens, R. C. Ligand Binding and Subtype Selectivity of the Human A(2A) Adenosine Receptor: Identification and Characterization of Essential Amino Acid Residues. *J. Biol. Chem.* **2010**, *285*, 13032–13044.

(65) Cristalli, G.; Lambertucci, C.; Marucci, G.; Volpini, R.; Dal Ben, D. A<sub>2A</sub> Adenosine Receptor and its Modulators: Overview on a Druggable GPCR and on Structure-Activity Relationship Analysis and Binding Requirements of Agonists and Antagonists. *Curr. Pharm. Des.* **2008**, *14*, 1525–1552.

(66) Floris, M.; Sabbadin, D.; Medda, R.; Bulfone, A.; Moro, S. Adenosiland: Walking through Adenosine Receptors Landscape. *Eur. J. Med. Chem.* **2012**, *58*, 248–257.

(67) Jiang, Q.; Van Rhee, A. M.; Kim, J.; Yehle, S.; Wess, J.; Jacobson, K. A. Hydrophilic Side Chains in the Third and Seventh Transmembrane Helical Domains of Human A<sub>2A</sub> Adenosine Receptors are Required for Ligand Recognition. *Mol. Pharmacol.* **1996**, *50*, 512–521.

(68) Jiang, Q.; Lee, B. X.; Glashofer, M.; Van Rhee, A. M.; Jacobson, K. A. Mutagenesis Reveals Structure-Activity Parallels between Human A2A Adenosine Receptors and Biogenic Amine G Protein-coupled Receptors. *J. Med. Chem.* **1997**, *40*, 2588–2595.

(69) Kim, J.; Wess, J.; Van Rhee, A. M.; Schöneberg, T.; Jacobson, K. A. Site-directed Mutagenesis Identifies Residues Involved in Ligand Recognition in the Human A2a Adenosine Receptor. *J. Biol. Chem.* **1995**, *270*, 13987–13997.

(70) Kim, S.-K.; Gao, Z.-G.; Van Rompaey, P.; Gross, A. S.; Chen, A.; Van Calenbergh, S.; Jacobson, K. A. Modeling the Adenosine Receptors: Comparison of the Binding Domains of A<sub>2A</sub> Agonists and Antagonists. *J. Med. Chem.* **2003**, *46*, 4847–4859.

(71) Ijzerman, A. P.; Von Frijtag Drabbe Künzel, J. K.; Kim, J.; Jiang, Q.; Jacobson, K. A. Site-directed Mutagenesis of the Human Adenosine A<sub>2A</sub> Receptor. Critical Involvement of Glu13 in Agonist Recognition. *Eur. J. Pharmacol.* **1996**, *310*, 269–272.

(72) Hino, T.; Arakawa, T.; Iwanari, H.; Yurugi-Kobayashi, T.; Ikeda-Suno, C.; Nakada-Nakura, Y.; Kusano-Arai, O.; Weyand, S.; Shimamura, T.; Nomura, N.; Cameron, A. D.; Kobayashi, T.; Hamakubo, T.; Iwata, S.; Murata, T. G-Protein-Coupled Receptor Inactivation by an Allosteric Inverse-Agonist Antibody. *Nature* **2012**, *482*, 237–240.